302
8-1-77

Lh. 1269

SAND-77-0938
Unlimited Distribution

OPTICAL PROPERTIES OF A SOLAR-ABSORBING MOLTEN SALT HEAT TRANSFER FLUID

W. D. DROTNING

DISTRIBUTION OF THIS DOCUMENT IS UNLIMITED

Prepared by Sandia Laboratories, Albuquerque, New Mexico 87115 and Livermore, California 94550 for the United States Energy Research and Development Administration under Contract AT (29-1)-789

June 1977

DISTRIBUTION OF THIS DOCUMENT IS UNLIMITED

Sandia Laboratories
energy report

SF 2900-QQB(3-74)

DISCLAIMER

This report was prepared as an account of work sponsored by an agency of the United States Government. Neither the United States Government nor any agency Thereof, nor any of their employees, makes any warranty, express or implied, or assumes any legal liability or responsibility for the accuracy, completeness, or usefulness of any information, apparatus, product, or process disclosed, or represents that its use would not infringe privately owned rights. Reference herein to any specific commercial product, process, or service by trade name, trademark, manufacturer, or otherwise does not necessarily constitute or imply its endorsement, recommendation, or favoring by the United States Government or any agency thereof. The views and opinions of authors expressed herein do not necessarily state or reflect those of the United States Government or any agency thereof.

DISCLAIMER

Portions of this document may be illegible in electronic image products. Images are produced from the best available original document.

Issued by Sandia Laboratories, operated for the United States Energy Research & Development Administration by Sandia Corporation.

NOTICE

This report was prepared as an account of work sponsored by the United States Government. Neither the United States nor the United States Energy Research & Development Administration, nor any of their employees, nor any of their contractors, subcontractors, or their employees, makes any warranty, express or implied, or assumes any legal liability or responsibility for the accuracy, completeness or usefulness of any information, apparatus, product or process disclosed, or represents that its use would not infringe privately owned rights.

SF 1004-DF (3-75)

Printed in the United States of America

Available from: National Technical Information Service
U.S. Dept. of Commerce
5285 Port Royal Road
Springfield, VA 22161

Price: Printed Copy $4.00 ; Microfiche $3.00

SAND-77-0938

OPTICAL PROPERTIES OF A SOLAR-ABSORBING MOLTEN SALT HEAT TRANSFER FLUID

W. D. Drotning

ABSTRACT

The optical absorption properties of a high temperature molten salt heat transfer fluid were measured from 0.35 μm to 2.5 μm using both hemispherical transmission and reflection techniques. This fluid has application as a direct-absorbing working fluid in a high temperature central receiver solar energy facility. The absorption spectrum of the pure molten fluid--a eutectic mixture of KNO_3, $NaNO_2$, and $NaNO_3$, known as Hitec (Du Pont tradename)--displays a fundamental absorption edge near 410 nm, which was found to shift to longer wavelength linearly with temperature. Throughout the remainder of the visible spectrum, the fluid is transparent. To enhance its solar absorption, particulate metallic oxides of Co or Cu were introduced into the fluid. Absorption spectra of these oxide particle suspensions in the molten salt were determined as a function of dopant concentration ranging from 0 to 0.1 wt% metal nitrate added to the Hitec. These measurements were carried out at 200°C under flow conditions to cause a homogeneous suspension of particles. Special transmission and reflection flow cells were designed and constructed to handle 200°C fluids. The suspended particles cause an additional optical absorption throughout the visible spectrum which is characteristic of the particular metallic oxide and closely follows a Beer-Lambert concentration dependence. The solar averaged absorption in a fixed layer thickness was calculated for various concentrations of the fluid-oxide mixtures. The fluid without oxide particles absorbs approximately 8% of the solar spectrum per cm of path length. Addition of 0.1 wt% of $Co(NO_3)_2 \cdot 6H_2O$ increases this absorption to approximately 90% per cm. Of the oxides studied, Co_3O_4 particle suspensions offer better solar absorption characteristics than CuO. Effects of particulate scattering on the measurements are discussed.

NOTICE
This report was prepared as an account of work sponsored by the United States Government. Neither the United States nor the United States Energy Research and Development Administration, nor any of their employees, nor any of their contractors, subcontractors, or their employees, makes any warranty, express or implied, or assumes any legal liability or responsibility for the accuracy, completeness or usefulness of any information, apparatus, product or process disclosed, or represents that its use would not infringe privately owned rights.

MASTER

DISTRIBUTION OF THIS DOCUMENT IS UNLIMITED

I. Introduction

With recent interest in utilizing solar insolation as a significant source of inexhaustible, clean energy, several schemes have emerged for large-scale electric power production from solar energy. Among these is the optical cavity system, commonly referred to as the "power tower" concept, first described by Baum et al.[1] and more recently by Hildebrandt and Vant-Hull[2]. In this concept, a mirror array is used to fucus sunlight through a windowless aperture into the bottom of a cylindrical cavity located at the top of a tower. In the cavity, the incident solar flux is converted to thermal energy and transported to a heat transfer fluid which is used in a high temperature electrical power generation system.

An advanced version of the central receiver concept is being studied at Sandia Laboratories[3], wherein the solar flux is absorbed directly into a heat transfer fluid flowing down the inside wall of the optical cavity. This method of energy transfer has several advantages over a receiver using water/steam in tubes, including lower surface temperature with consequent reduction of radiative and convective heat losses; avoidance of thermal stress and heat transfer limitations; decreased problems of hot spots caused by high flux concentrations in the cavity; simpler control, lower weight, and lower cost; and a better thermodynamic match with thermal storage. In addition, a higher pressure, higher temperature steam turbine can be utilized, resulting in considerably higher overall system efficiency than can be achieved by the current systems using water/steam receivers[3].

An essential parameter in the analysis of energy transfer and efficiency within the optical cavity is the optical density of the directly-absorbing heat transfer fluid[4,5]. In this study, we report the experimental results of optical studies on the solar absorption characteristics of such a fluid. To enhance the solar absorptivity, dopants are introduced into the fluid. Most studies of the optical properties of doped fused salt systems deal with the spectroscopy of transition metal ions in solution[6,7]. However, the use of a molten salt as a heat-transfer fluid in a solar central receiver facility requires 1) long-term dopant stability at high temperatures ($\sim 500°C$) in a highly-oxidizing environment, and 2) broad-band solar absorption; both criteria eliminate the use of homogeneous solutions to darken the heat transfer fluid. Instead, the doping technique studied here utilizes particulate metallic oxides suspended in the fluid. The oxide particles offer both broad-band spectral absorption and relatively high absorption coefficients throughout their absorption, as well as thermal stability at high temperatures.

II. Sample Characterization

The primary molten salt used in this study is the eutectic mixture of KNO_3, $NaNO_2$, and $NaNO_3$, in proportions 53-40-7 wt% (m.p. 142°C).[8] This salt was mixed from reagent-grade components and formed by heating in air to 400°C. While molten the salt is a pale yellow color. (This eutectic salt mixture will be referred to as "Hitec", a Du Pont tradename, throughout this report. Commercial-grade Hitec, as received from Du Pont, produces a thick foam on the surface of the melt, as well as some evidence of a brown scum. This material was judged too contaminated for optical measurements.)

Because of long-term decomposition of nitrite to nitrate in the Hitec melt at elevated temperatures[9], the binary eutectic nitrate salt was studied, as well. The composition is 58 wt% KNO_3-42 wt% $NaNO_3$; the melting point is 222°C.[10] The binary nitrate melt does not absorb visible radiation.

The technique used to darken the molten salt is to add a small amount (~ .05 wt%) of hydrated transition metal nitrate to the Hitec melt. At 300-400°C, the metal ions react rapidly with the melt (probably the nitrite) forming a suspension of black metallic oxide particles. Preliminary studies[3] using this technique showed Co and Cu oxides remained in suspension the longest of those studied, and would therefore be the most suitable in the proposed application. Hence, these transition metal oxides were studied here. No differences in the resulting optical spectra were observed using nitrates or chlorides (e.g., $Cu(NO_3)_2 \cdot 3H_2O$ or $CuCl_2$); the hydrated metal nitrates, either $Cu(NO_3)_2 \cdot 3H_2O$ or $Co(NO_3)_2 \cdot 6H_2O$, were used in this study. The oxide concentration in the melt is reported in terms of the wt% of metal nitrate added to the melt.

To dope the binary nitrate eutectic similarly, 0.5 wt% $NaNO_2$ was added to cause formation of the metallic oxide, since no oxide was formed at 400°C in the nitrate eutectic alone.

The particulate metallic oxides were separated from the salt for analysis by dissolving the doped (frozen) salt in distilled H_2O. This solution was repeatedly centrifuged, decanted, and diluted until the dissolved salt was removed. The remaining oxide powder was analyzed by X-ray diffraction for composition and by scanning electron microscopy (SEM) for particle size estimation. The X-ray analysis showed Co_3O_4 was formed from $Co(NO_3)_2 \cdot 6H_2O$ in Hitec, while CuO was formed by addition of cupric nitrate to Hitec. The SEM analysis yielded particle sizes of 0.06-0.15 μm for the CuO particles, and 0.03-0.10 μm for Co_3O_4. These particles tend to cluster together in the melt, however, so that much larger oxide chunks form and eventually settle to the bottom of the melt. Continuous stirring of the fluid is therefore required to maintain the suspension. The exact particle sizes while in suspension (flowing) may differ from the SEM analysis. Left unstirred, the Co_3O_4 particles remained suspended longer than CuO (~ 1 hour vs. minutes[3]) probably due to the smaller size of the Co_3O_4 particles.

III. Optical Measurement Techniques

The experimental techniques used in this study had several common features. First, all measurements were made at melt temperatures of 200 ± 5°C, except where noted. Most measurements were made using a Beckman DK-2 spectroreflectometer with a 6" diameter integrating sphere detector coated with $BaSO_4$ paint. Inlet (transmission) and exit (reflection) ports were nominally 2 cm diameter holes. The spectral range observed was 0.35-2.5 μm, using a combination of detectors; this wavelength range spans approximately 99% of the solar spectrum of air mass two. The use of an integrating sphere in the detection system allows hemispherical (2π steradians) detection of transmitted or reflected radiation, depending on the mode of operation.

To maintain a suspension of oxide particles in the fluid under study, it was necessary to continuously pump the fluid vertically past the optical measurement port. To do this, special flow cells (transmission and reflection) were constructed, capable of handling 200°C fluids. An Eastern Industries Model B-1 liquid circulating pump with a 316 stainless steel impeller and housing was used. The entire plumbing circuit, including reservoir, copper tubing, and pump, was wrapped with electric rope heaters. Fluid temperature was monitored using a type J thermocouple; the heater circuits were controlled by a temperature regulator. A motor speed control was used to adjust the flow rate of the liquid through the system; typical operating flows were on the order of 10 ml per second.

1) Transmission Measurements.

The primary optical arrangement used in this study is shown schematically in Fig. 1(a). This geometry is used to measure the so called normal hemispherical transmission, τ (0°; 2π), using radiation normally-incident on the sample, and collecting transmitted radiation over the forward hemisphere (2π steradians). Radiation transmitted into the entire forward hemisphere can be divided into two components, normal (i.e., radiation detected over a small solid angle in the direction of the incident beam), and diffuse (everything else). Experimentally, the normal component was determined by the size of the exit port of the integrating sphere; this component subtends an included angle of 7.6°, representing 0.2% of the area of the forward hemisphere.

Special transmission cells were designed and constructed to allow the high temperature fluid to flow past the optical beam in a thin layer as near as possible to the integrating sphere. The transmission flow cell is shown in Fig. 2. Internal pathlengths of 3 and 6 mm were used for reference and sample cells, respectively, when a reference cell was used. Both entrance and exit flow ports were located on one side of the cell, allowing the other side to be placed flush against the integrating sphere detector during the measurements. The cell was constructed of Pyrex optical windows and tubing. The pump and plumbing seals limited temperatures to

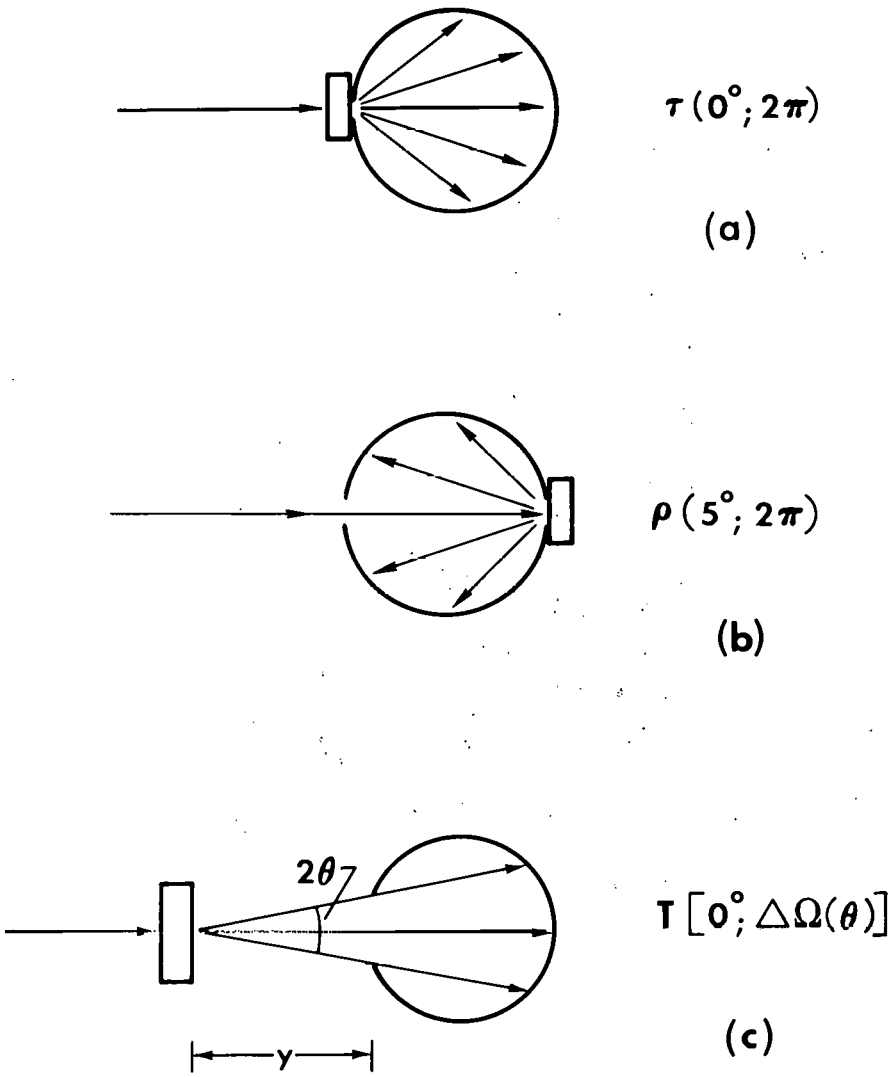

Figure 1. Schematic optical measurement geometries.

a) Normal incidence--hemispherical transmission;
b) Near-normal incidence--hemispherical reflectance;
c) Normal incidence--transmission into a solid angle around normal.

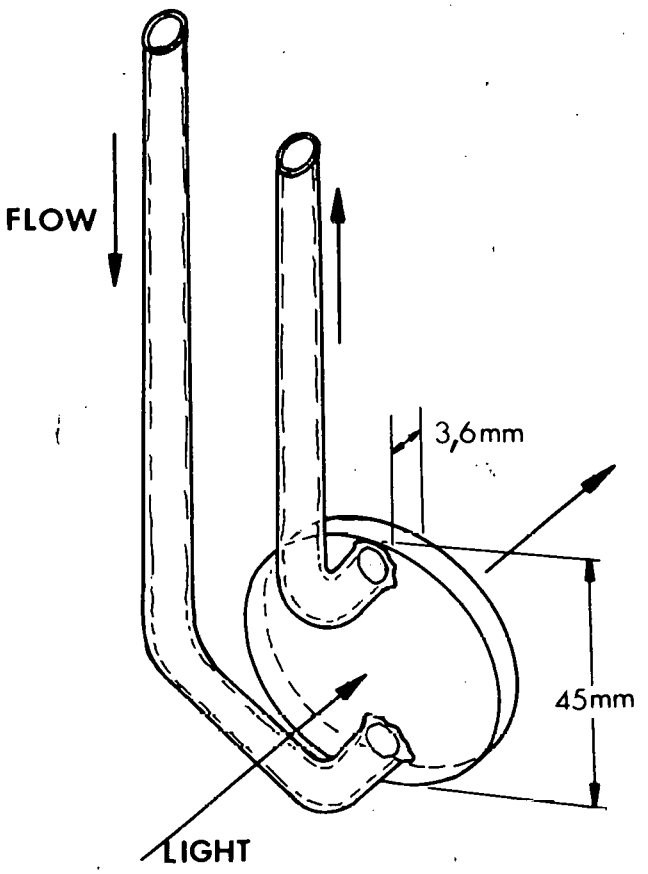

Figure 2. Transmission flow cell for high temperature fluids. Dimensions in direction of light beam are for reference and sample cells, respectively.

below 300°C. Thermal transfer to the integrating sphere detection system (both conductive and radiative) also becomes significant at about 300°C, and further limits the temperature range.

All transmission measurements were calibrated to a spectral curve of 100% transmission through the system, measured using no cells in either reference or sample beam.

2) Reflection Measurements.

In principle, the optical absorption coefficient of an absorbing material may be obtained from either reflection or transmission measurements. While the transmission technique is more direct from an analytical standpoint, the reflection technique was also used in this study for two reasons. (1) The reflection mode of measurement more closely resembles the actual central receiver configuration of a fluid layer flowing over an opaque substrate. This measurement technique allows the possibility of varying the metallic reflecting substrate in order to determine the reflectance of specific layer-substrate interfaces. (2) Both transmission and reflection measurements are desirable, since light scattering by suspended particles may affect the apparent absorption differently in the two measurement modes. (For example, backscattered radiation is collected in the reflection mode, and lost in the transmission mode.)

The reflection measurements were made using the optical arrangement shown schematically in Fig. 1(b). The measured quantity is $\rho(5^\circ; 2\pi)$, that is, the overall reflectance, detected hemispherically, from a sample illuminated with approximately normally-incident radiation. (The slight deviation from normal incidence allows containment of the specularly-reflected component in the integrating sphere detector.)

A reflection cell was designed to allow the measurement of the hemispherical reflectance from a 200°C fluid flowing across a reflecting metallic substrate. A cross-section of this cell is shown in Fig. 3. A copper block formed the body of the cell and was heated with inserted cartridge heaters. The copper piston (diameter 5.08 cm) supported the reflector substrate, and could be moved within the block to vary the fluid layer dimension perpendicular to the face of the substrate. The metallic reflector substrate (2.54 cm x 3.81 cm x .16 cm, 316 SS) was a specular reflector over the solar spectrum. During the optical measurement, the fluid flowed continuously between the quartz window and the substrate, passing the reflectance port of the integrating sphere detector. A mechanical wiper was used to wipe away particles which settled on the substrate during the course of a measurement. Typical fluid layer thicknesses used were 0.18 cm and 0.30 cm. (Reflection measurements for two layer thicknesses are necessary to unfold the data.) The liquid seals used in the reflection cell limit its temperature to 250°C.

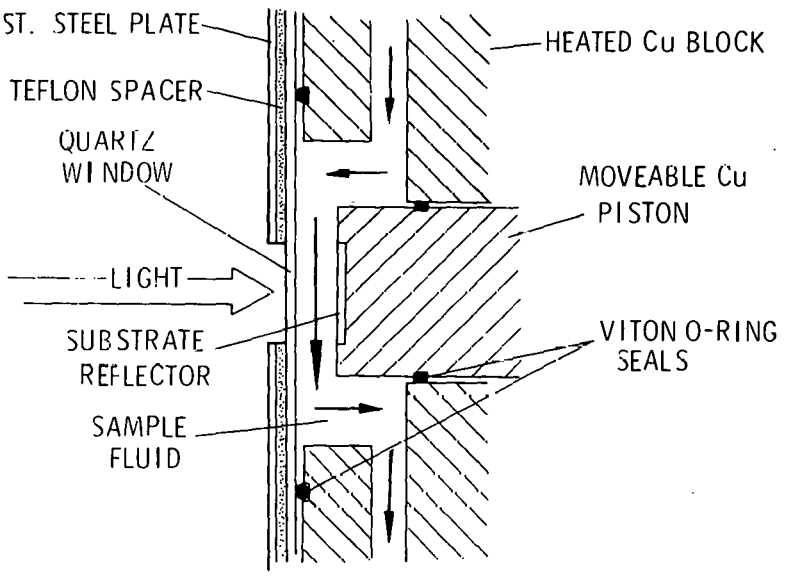

Figure 3. Cross-section of high temperature flow cell for reflection measurements (not to scale).

The reflection measurements were referenced to the reflectance of a $BaSO_4$ powder. In turn, the $BaSO_4$ powder reflectance was measured against a Vitrolite glass whose absolute reflectance was given by an NBS calibration. The net result is that the reflection measurements were corrected to absolute values, traceable to NBS standards.

3) Scattering Distribution.

The intensity distribution of scattered radiation in the forward hemisphere was measured using the transmission flow cell and a special optical arrangement, shown schematically in Fig. 1(c). A collimated beam of monochromatic radiation (λ = 0.6746 μm, Kr laser) was normally incident on the doped fluid suspension circulating through the flow cell. Transmitted radiation was measured by a 4" diameter integrating sphere detector with a fixed aperture (1.27 cm diameter), as a function of the distance y between sample cell and aperture. The aperture size and distance y define an included angle in the forward direction over which radiation is detected. The resulting curve of percent transmission vs. included angle 2θ may be differentiated to yield the transmission beam profile at various θ (assumed axially symmetric about the incident beam direction).

IV. Analysis of Data

The material under study is an absorbing-scattering fluid composed of a suspension of metallic oxide particles in a fluid layer. Many theories which describe absorbing-scattering media are phenomenological and either describe single-scattering cases or multiple-scattering in tightly-packed particle layers.[11] For the case of multiple-scattering in an extended, partially-transparent layer (the problem considered here), available treatments become extremely complex. Frequently, a number of parameters are involved in a complete description.[11] Besides being very difficult to determine experimentally, a large number of descriptive parameters are not clearly useful in any operational sense.

We analyze the optical data on the fluid under study in terms of an absorbing layer of known thickness x, and absorption coefficient α, which depends on type and concentration of dopant, as well as wavelength. In first order, we include scattering in the treatment by using hemispherical detection of either transmitted or reflected radiation. The absorption coefficient thus obtained is an operational one, and is useful in determining the actual energy transferred to the fluid without a knowledge of the details of the scattering process. The validity of this analysis will be discussed in a later section.

An additional assumption used here is that the index of refraction n is solely due to the molten salt, and can be deduced from the literature. The refractive index of the binary eutectic KNO_3-$NaNO_3$ (53-47 mole %) was measured by Jindal,[12] and found to be $n = 1.4740 - (1.6 \times 10^{-4})\ T(^\circ C)$ in the range 258-356°C. Others[13]

have found that binary molten salts have refractive indices linearly dependent on the composition of the mixture, varying between the component material values. This can be expected to hold for ternary mixtures, as well. Using Bloom and Rhodes' component values,[13] one would expect an index of refraction for molten Hitec of approximately $n = 1.476 - (10^{-4})\ T(°C)$ at the Na D line, or $n \approx 1.456$ at 200°C.

For a layer of thickness x and wavelength-dependent absorption coefficient $\alpha(\lambda,c)$, the percentage of transmission through the layer is determined by

$$T(\lambda) = e^{-\alpha(\lambda,c)x} \quad , \tag{1}$$

where c is the dopant concentration. When two cells are used in a double-beam transmission measurement, $T(\lambda)$ is measured directly, since interface reflections common to both sample and reference cells are equivalent, and essentially cancel each other. The layer thickness x is then the difference in pathlength of the two cells, and (1) yields $\alpha(\lambda,c)$ directly.

For a transmission measurement using no reference cell, one obtains the external transmittance, which includes not only the exponential attenuation given by Eq. (1), but also the transmission losses due to interface reflections. The index n of Pyrex is 1.474 at the Na D line. Thus, the glass/Hitec interface reflection is[11]

$$R = \left(\frac{n_1 - n_2}{n_1 + n_2}\right)^2 = 3.8 \times 10^{-5} \quad , \tag{2}$$

which is negligibly small. The air/glass interfaces each contribute a reflectance of R = 0.037. A valid approximation relates the external (measured) transmission to the internal (sample) transmission by

$$T_{ext} = T_{int}\ (1-2R) \quad , \tag{3}$$

correct to first order in R. Using (3), the measured values are converted to internal transmission vs. wavelength, and $\alpha(\lambda,c)$ is again found from (1).

The absorption coefficient $\alpha(\lambda,c)$ is determined less directly from the reflection measurements. The optically-measured region of the reflectance cell is schematically represented in Fig. 4(a). Light is incident on an optical window (in this case, fused silica) and is then transmitted through the fluid layer and reflected from the substrate surface. The refractive index of fused silica at 200°C is approximately 1.461[14] for the Na D line, giving a window/fluid reflection of $\sim 3 \times 10^{-6}$, again negligible. By treating the absorbing-scattering fluid as a simple absorbing layer, as discussed above, the model in Fig. 4(a) is reduced to that shown in Fig. 4(b), consisting of an absorbing layer of thickness x, and reflections at two interfaces, R_1 and R_2.

Assuming no attenuation in the window, and normally-incident radiation, the overall reflectance ρ of the configuration in Fig. 4(b) is found from the familiar

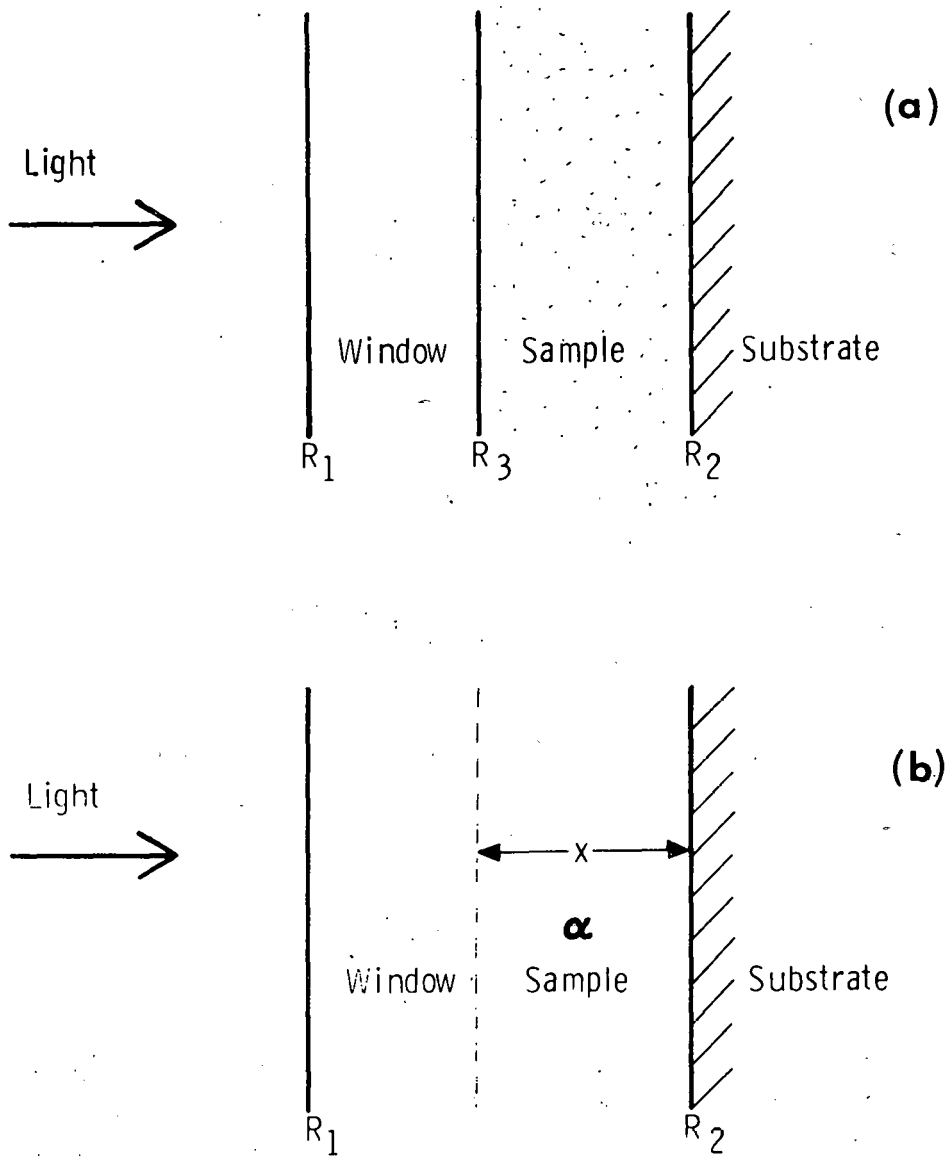

Figure 4. Cross-sectional schematic of reflection cell.

a) Actual interfaces;
b) Simplified model of a).

bouncing-ray technique, discussed in several texts[11-15]. The result is

$$\rho = R_1 + \frac{R_2(1-R_1)^2\, T^2}{1 - R_1 R_2\, T^2} \quad , \tag{4}$$

where T is given by (1). From reflection spectra $\rho_a(\lambda)$ and $\rho_b(\lambda)$ at two layer thicknesses x = a and x = b, the absorption coefficient is given by

$$\alpha(\lambda,c) = \frac{1}{2(b-a)}\ \ln\left[\left(\frac{\rho_a - R_1}{\rho_b - R_1}\right)\left(\frac{\rho_b R_1 - 2R_1 + 1}{\rho_a R_1 - 2R_1 + 1}\right)\right] \quad . \tag{5}$$

The air/window interface reflection R_1 is measured independently. The fluid/substrate reflectance is given by

$$R_2 = \left(\frac{\rho_a - R_1}{\rho_a R_1 - 2R_1 + 1}\right) e^{2a\alpha} \quad . \tag{6}$$

From the spectral absorption coefficient $\alpha(\lambda,c)$, found either by transmission or reflection, it is useful to calculate the energy absorption in a fluid layer of thickness x, averaged over the solar spectrum of air mass m. This quantity is defined by

$$A_m(x,c) = \frac{\int S_m(\lambda)\left[1 - e^{-\alpha(\lambda,c)x}\right] dx}{\int S_m(\lambda)\, d\lambda} \quad , \tag{7}$$

where $S_m(\lambda)$ is the spectral distribution of the solar intensity through an air mass m[16]. The quantity in (7), $[1 - e^{-\alpha(\lambda,c)x}]$, represents the energy attenuation of an optical beam of wavelength λ by a fluid layer of thickness x, and does not include reflections at the fluid interfaces.

Values of $A_m(x,c)$ were numerically integrated on a digital computer according to Eq. (7). Approximately 2% of the solar spectrum was not used in the numerical integration, due to lack of data on $\alpha(\lambda)$ in the infrared beyond 2.5 μm, and in the region of the molten salt uv cutoff, roughly 0.41 μm to 0.425 μm. Below 0.41 μm, in the Hitec uv absorption band, $\alpha(\lambda) \sim 10^3\ \mathrm{cm}^{-1}$,[17] so that the contribution to $A_m(x,c)$ at these wavelengths is a maximum, i.e., $(1 - e^{-\alpha x}) \approx 1$, for $x > 10^{-2}$ cm.

V. Results and Discussion

1) Spectral Absorption Properties.

Absorption spectra were measured for Co_3O_4 and CuO in Hitec as a function of the concentration of dopant added (hydrated transition metal nitrate). No observed spectral differences were seen using $CuCl_2$ as the starting salt instead of copper nitrate, and no significant differences were seen between the absorption spectra determined from transmission or reflection measurements. Several methods of introduction of the dopant to the melt were tried; in all cases, the metal ion was rapidly oxidized and formed particles in suspension. Doping of Hitec was also achieved using nitrate or chloride salts of nickel, chromium, and iron; oxide particles again were formed, but settling of the particles occurred rapidly, and these materials were not examined further.

Typical transmission spectra are shown in Figs. 5, 6, and 7, for two concentrations of cobalt nitrate and one of copper nitrate in Hitec at 200°C, showing both hemispherical and diffuse spectra (percent transmission vs. wavelength). The solar-averaged (m = 1) transmission is also reported.

Typical absorption spectra calculated from transmission measurements are shown in Fig. 8 for Co_3O_4 and CuO in Hitec, as well as for pure Hitec. The undoped molten salt is essentially transparent throughout the solar spectrum, with the exceptions of the strong absorption in the near uv which causes the pale yellow color of the melt, and two spectral bumps in the infrared. The latter (small band near 2.0 μm and a band with $\alpha \sim 1.5\ cm^{-1}$ near 2.5 μm) appear to be caused by dissolved H_2O in the melt.

The introduction of the oxide dopants into the salt melt increases the absorption, particularly in the visible (both CuO and Co_3O_4 appear black). In the case of Co_3O_4, there is a strong absorption throughout the visible to about 0.85 μm, and an additional absorption band from 1.2 to 1.6 μm. For CuO, only a single band appears, extending through the visible to about 0.8 μm.

The reflection measurements also yield the spectral dependence of R_2, the fluid/substrate interface reflectance, given by Eq. (6). The $R_2(\lambda)$ spectra showed a wavelength dependence similar to that measured for the air/substrate reflectance, though reduced in value consistent with less refractive index (real part) mismatch in the fluid/substrate case versus the air/substrate case.

In addition to the X-ray analysis of the oxide stoichiometry, a spectroscopic analysis was made and is shown in Fig. 9. These spectra show the log of the remission function f(R) calculated from hemispherical reflection measurements of packed oxide powders at room temperature. The remission function[11]

$$f(R) - \frac{(1-R)^2}{2R} \qquad (8)$$

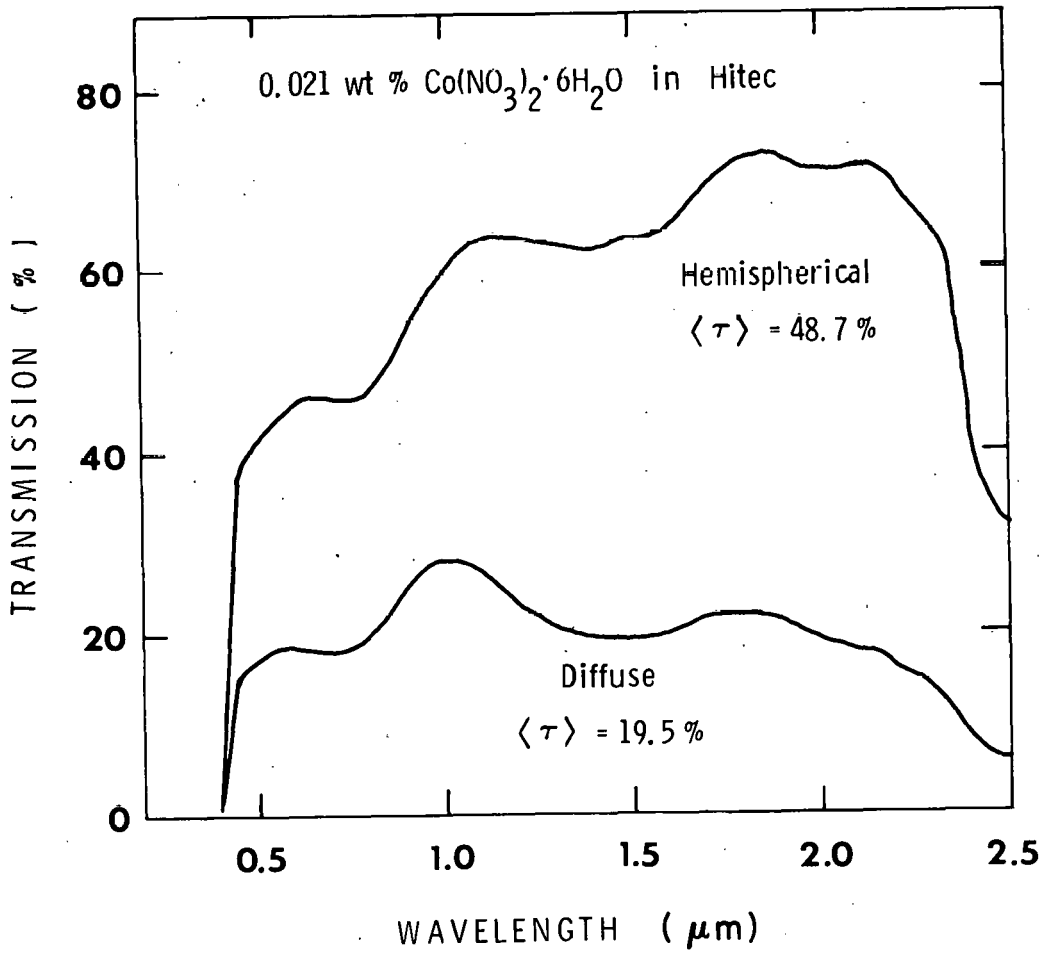

Figure 5. Percent transmission (hemispherical and diffuse) versus wavelength for Co_3O_4 in Hitec at 200°C. Oxide formed by addition of 0.021 wt% $Co(NO_3)_2 \cdot 6H_2O$ to Hitec. Cell pathlength was 6.9 mm. Solar-averaged percent transmission $\langle \tau \rangle$ is shown for each spectrum. The diffuse transmission spectrum is the hemispherical transmission minus that transmitted in a narrow cone (included angle 7.6°) around the normal.

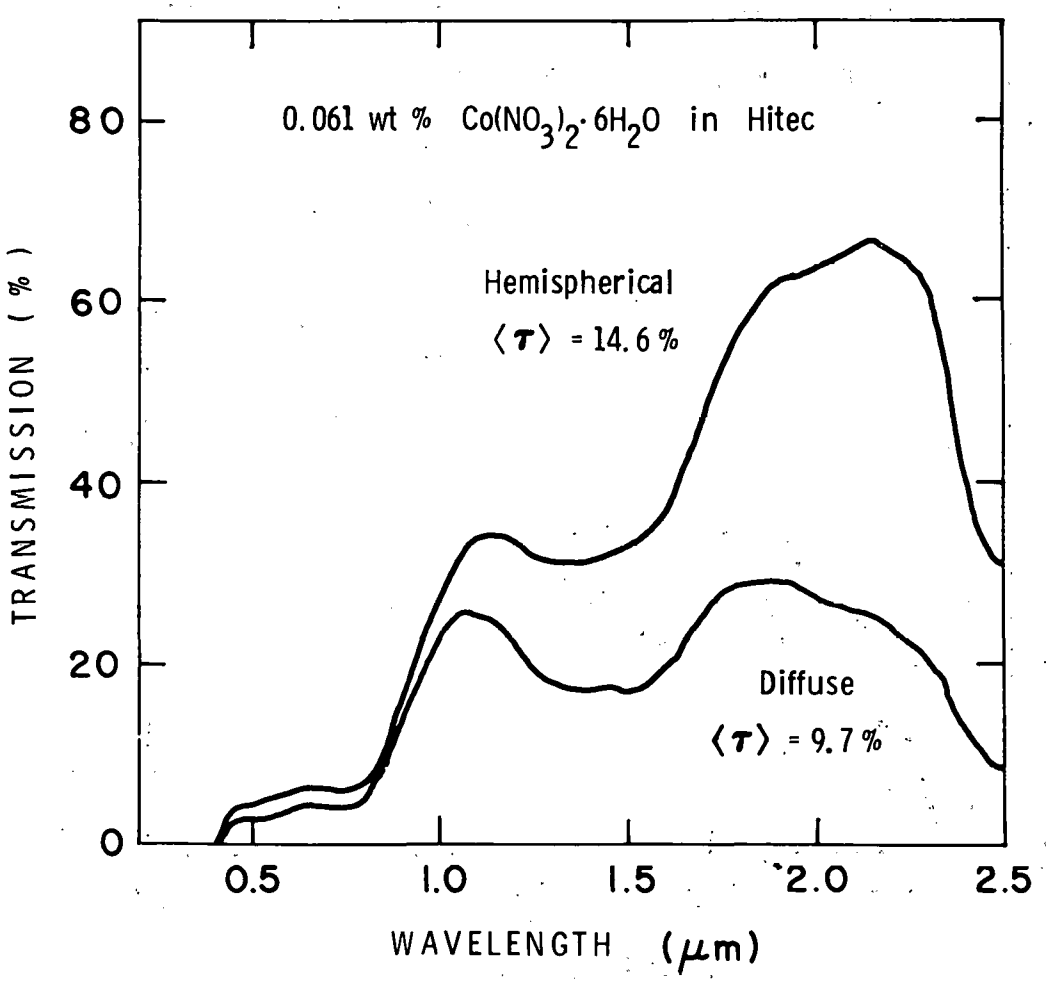

Figure 6. Percent transmission versus wavelength for Co_3O_4 in Hitec at 200°C, formed by addition of 0.061 wt% $Co(NO_3)_2 \cdot 6H_2O$ to Hitec. See additional notes to Fig. 5.

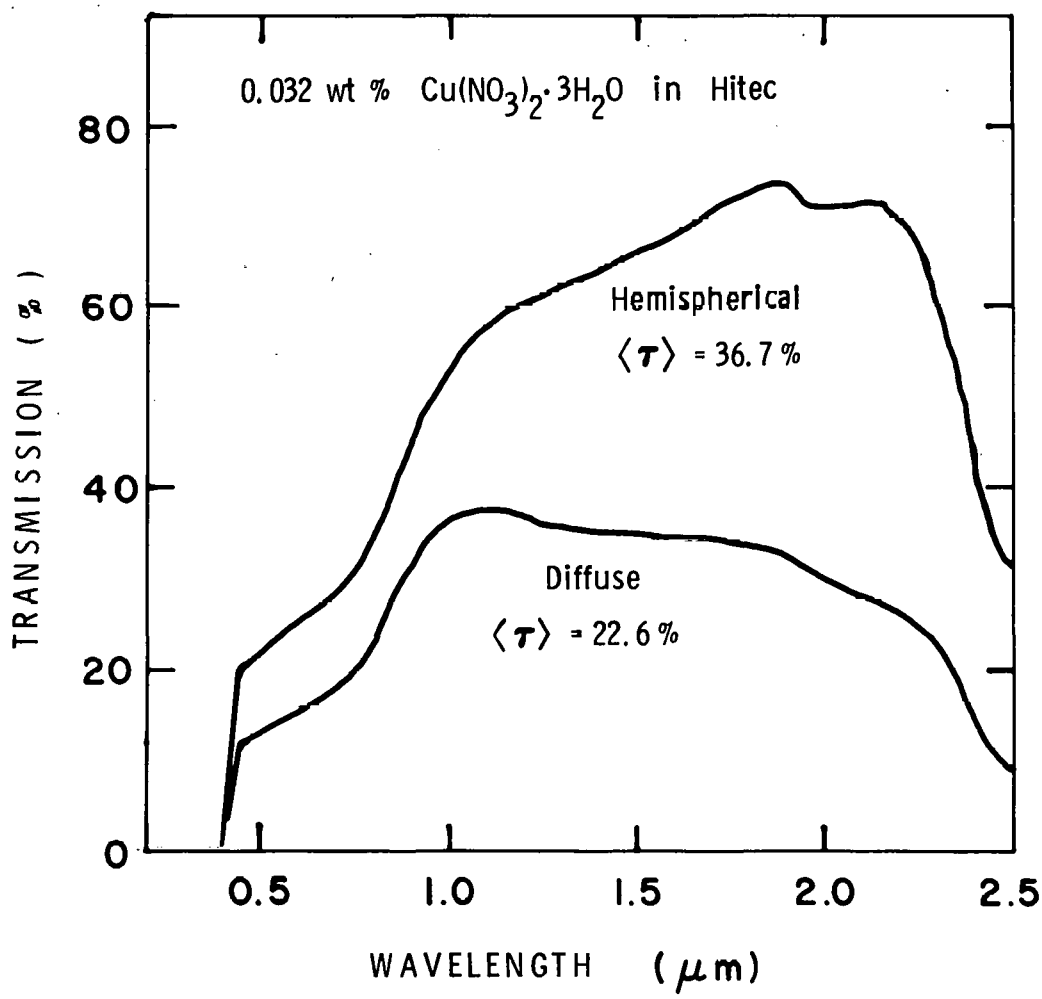

Figure 7. Percent transmission versus wavelength for CuO in Hitec at 200°C, formed by addition of 0.032 wt% $Cu(NO_3)_2 \cdot 3H_2O$ to Hitec. See additional notes to Fig. 5.

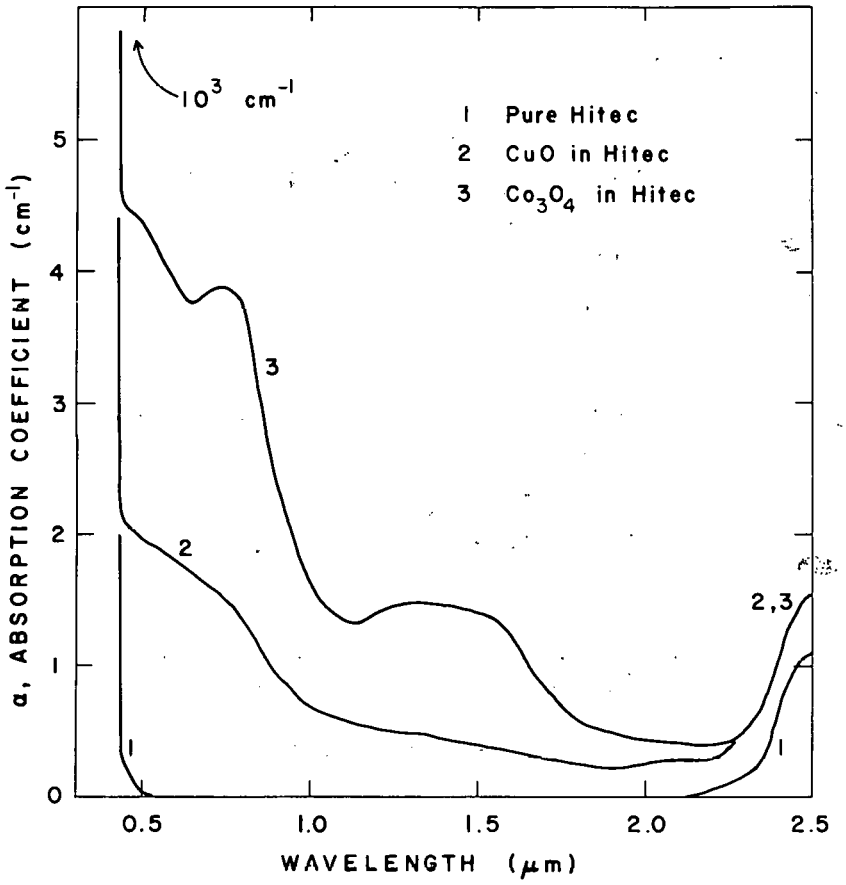

Figure 8. Absorption coefficient versus wavelength for pure Hitec (1), CuO (2), and Co_3O_4 (3) in Hitec, all at 200°C. Calculated from hemispherical transmission measurements. Dopant concentration of (2) is 0.032 wt% copper nitrate in Hitec; (3) is 0.061 wt% cobalt nitrate in Hitec. (Concentrations shown are intentionally unequal for graphical purposes.)

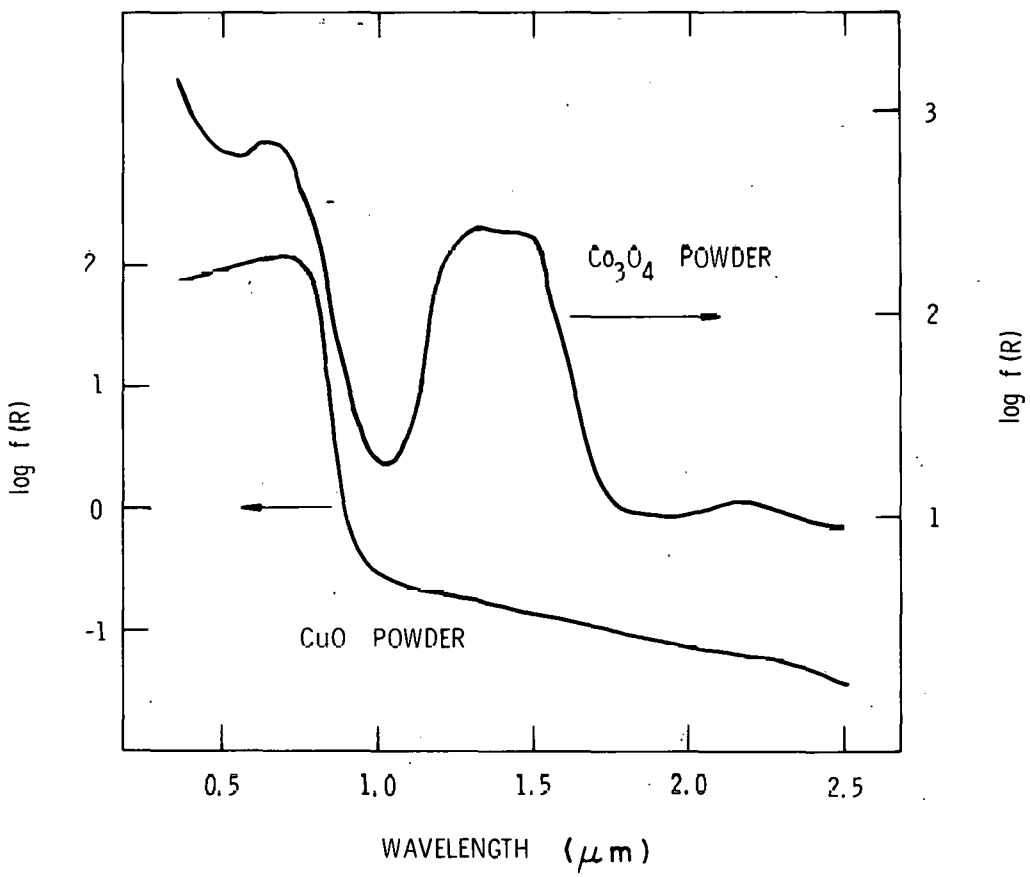

Figure 9. Log remission function f(R) versus wavelength for packed metallic oxide powders at room temperature. Determined by hemispherical reflection measurements and equation (8).

is related to the absorption coefficient α; the curves in Fig. 9 can be thought of as absorption spectra for opaque, absorbing powders. These spectra show absorption bands similar to those appearing in the doped melts. The sharp cutoffs near 0.8 μm are fundamental absorption edges for these oxides.

Figure 10 shows the same absorption spectra as in Fig. 8, but plotted on an abscissa linear in percentage solar spectrum, and thus non-linear in wavelength. This solar-weighted plot dramatically shows the enhancement to the solar absorption caused by oxide particle doping of the molten salt, as well as the insignificance of the H_2O absorption.

The strength of the optical absorption varies with concentration of dopant as well as with wavelength. For liquid solutions in which a particular concentration of dopant is responsible for the optical attenuation, one can define an extinction coefficient ϵ which depends only on the type of dopant and the wavelength of radiation, but not on the concentration c of dopant in solution. In this case, one has the Beer-Lambert relation

$$\alpha(\lambda,c) = \epsilon(\lambda)c + \alpha_s(\lambda) \quad , \tag{9}$$

where $\alpha_s(\lambda)$ is the absorption due to the solvent. We can apply this relationship to the case of absorbing particles suspended in a fluid.

Figure 11 shows the absorption coefficient of Co_3O_4 in Hitec at two wavelengths as a function of the amount of cobalt nitrate added to the melt. The lines are shown to indicate a Beer-Lambert dependence as in (9). Data from both transmission and reflection are included. In spite of the data scatter, the Beer-Lambert relation appears to describe the concentration dependence, except for a slight non-linear effect at the high dopant levels.

To characterize a given type and concentration of dopant, the solar-averaged quantity $A_2(1\ cm,c)$ was calculated for each spectrum, as defined in (7). The resulting value of $A_2(1\ cm,c)$, between 0 and 100%, indicates the percent of the solar spectrum (m = 2) which is absorbed in a fluid layer 1 cm thick. (This holds for normally-incident radiation, and does not include reflective losses at the air/fluid interface in an actual application.) Values of $A_2(1\ cm,c)$ are shown in Figs. 12 and 13 for Co_3O_4 and CuO, respectively. These graphs show $A_2(1\ cm,c)$ vs. amount c of metal nitrate added to the Hitec melt. For pure Hitec, $A_2(1\ cm,0)$ = 8.3% at 200°C. Results from both transmission and reflection are shown, and appear to show no discrepancies between the two types of measurements. For $\geq$ 0.08 wt% cobalt nitrate in Hitec, the solar-averaged absorption is $\geq$ 90% per cm of fluid. For equivalent wt% dopant added, the CuO absorbs slightly less, consistent with the differences in spectral structure, as shown in Figs. 8-10.

Also shown in Fig. 12 are data for the doped binary eutectic KNO_3-$NaNO_3$. (These values are for melts at 325°C.) The binary nitrate is clear in the melt; its uv cutoff is approximately 0.05 μm lower than the Hitec cutoff. As a result,

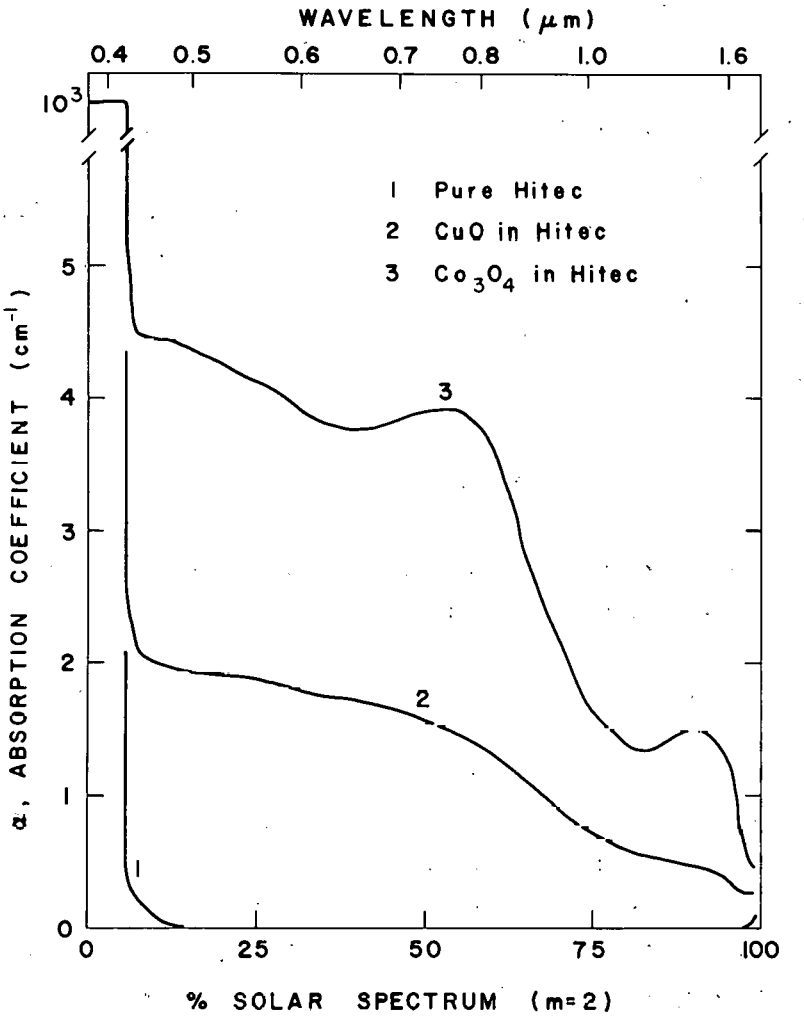

Figure 10. Absorption coefficient versus percent solar spectrum (air mass two) for pure Hitec (1), CuO (2), and Co_3O_4 (3) in Hitec, all at 200°C. Same spectra as in Fig. 8, except plotted on solar-weighted abscissa.

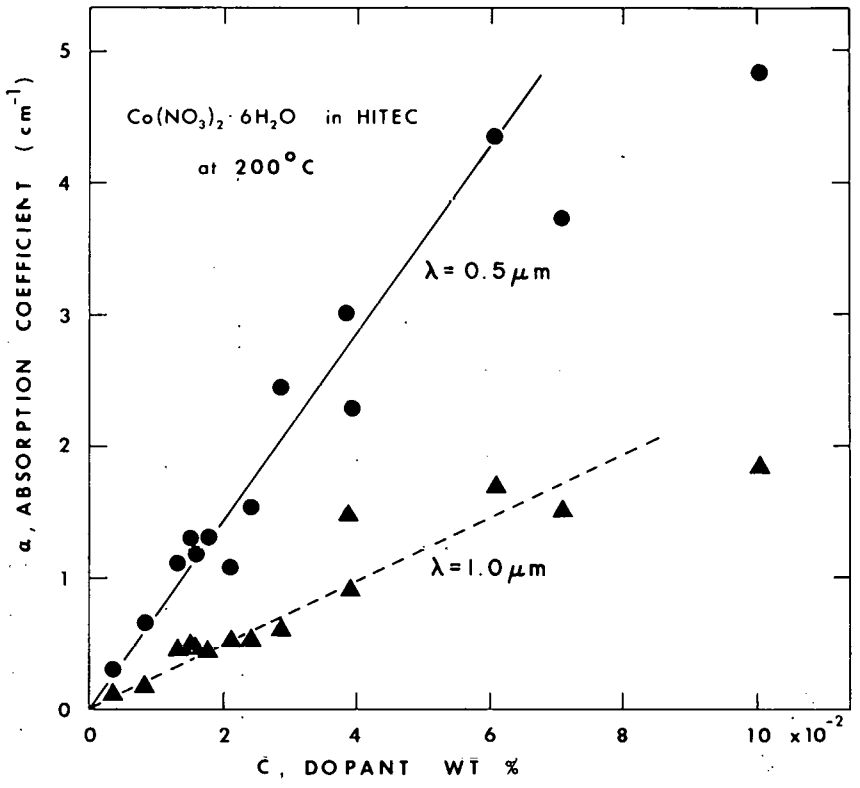

Figure 11. Absorption coefficient at selected wavelengths for Co_3O_4 in Hitec at 200°C versus dopant concentration (wt% cobalt nitrate in Hitec). Values from both hemispherical transmission and reflection techniques are included. Straight lines indicate a Beer-Lambert dependence.

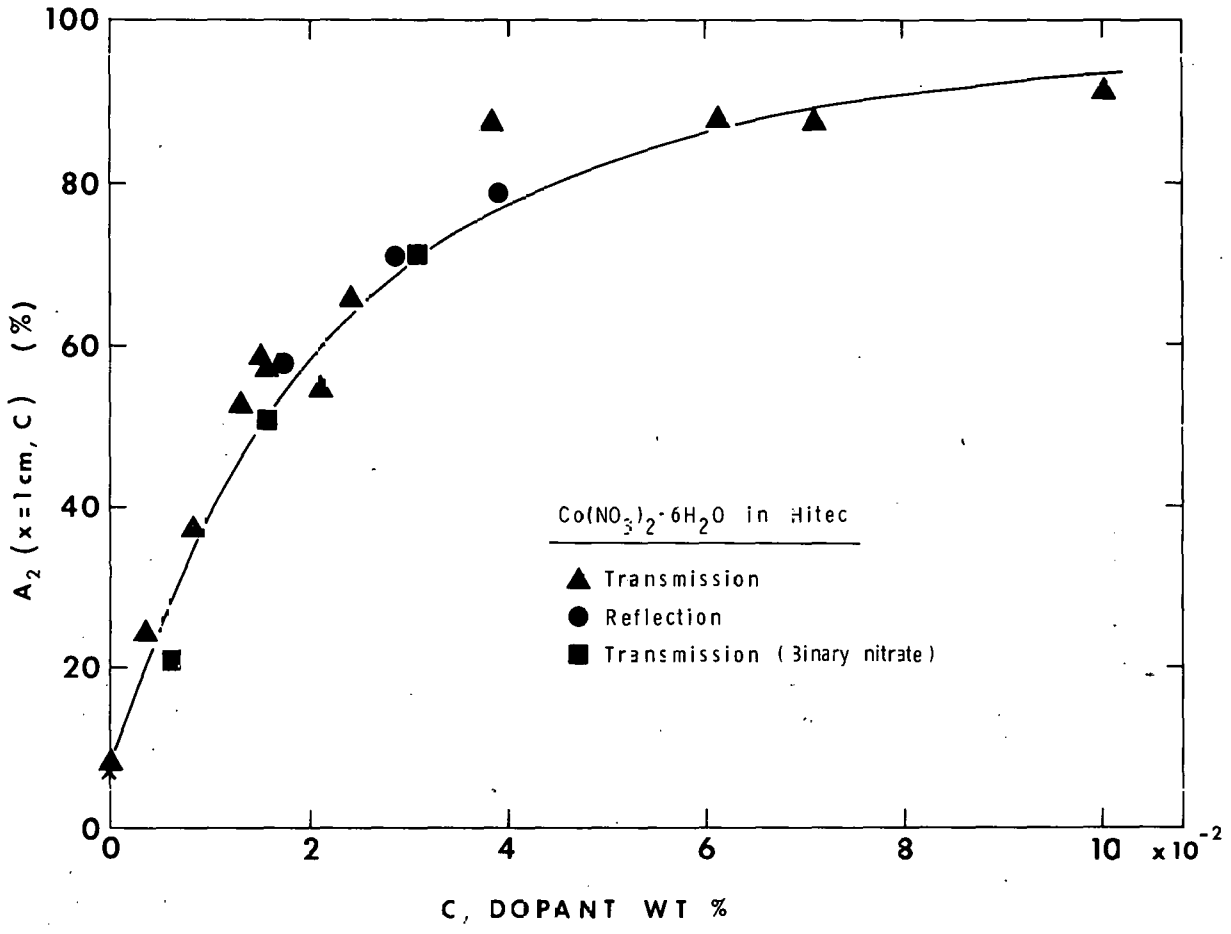

Figure 12. Solar-averaged (m = 2) percent absorption by Co_3O_4 in a 1 cm fluid layer of Hitec at 200°C versus dopant concentration (wt% cobalt nitrate added to Hitec). Transmission and reflection results shown. Also shown is percent absorption by Co_3O_4 in the molten binary eutectic salt (at 325°C). Curve is a predicted concentration dependence, discussed in text.

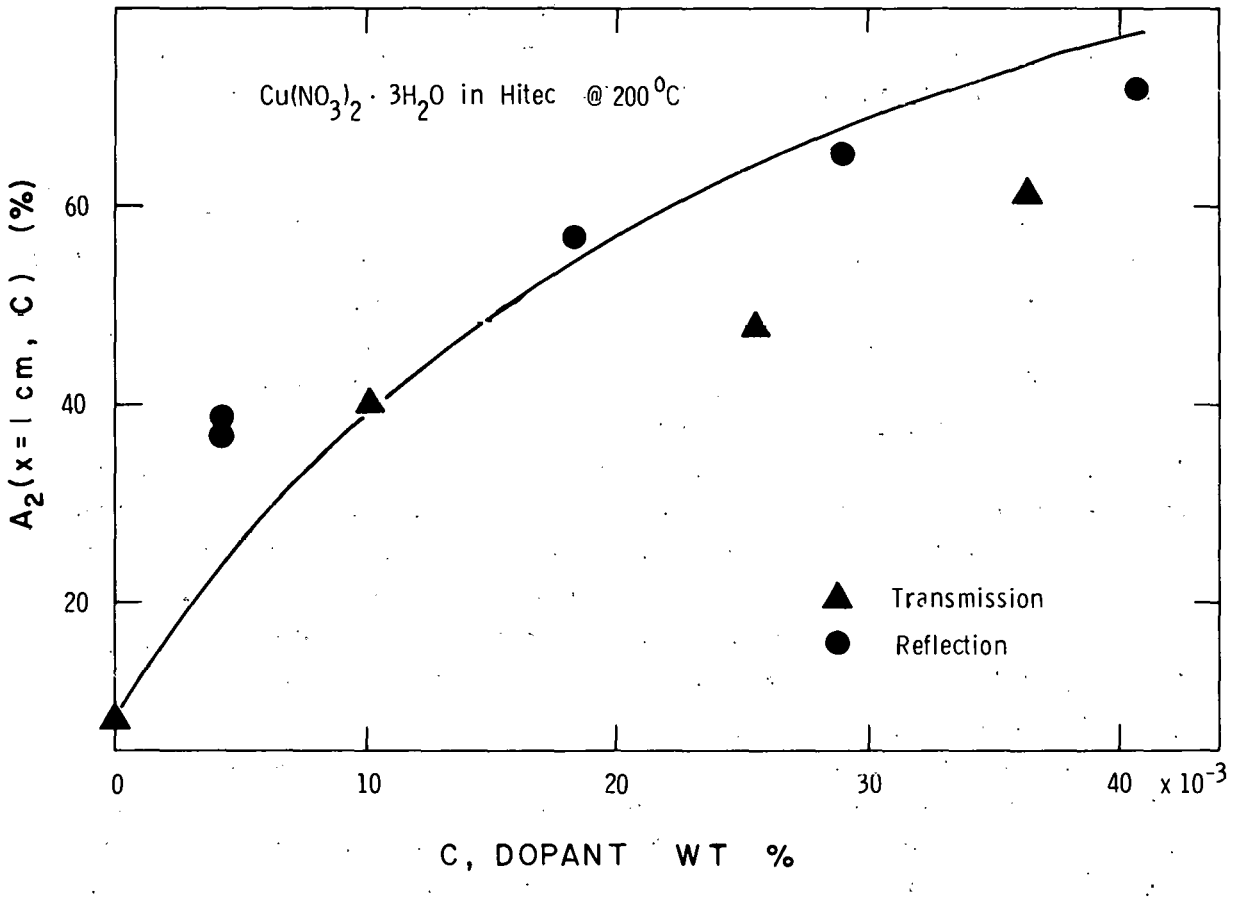

Figure 13. Solar-averaged (m = 2) percent absorption by CuO in a 1 cm fluid layer of Hitec at 200°C versus dopant concentration (wt% copper nitrate added to Hitec). Transmission and reflection results shown. The curve is a predicted concentration dependence, discussed in text.

A_2(1 cm,0) for the pure binary is about 3%. Since the pure molten salts (Hitec or binary nitrate) differ only slightly in their overall solar absorption and these values are small, one expects little difference in A_2(1 cm,c) between doped Hitec and the doped binary eutectic. This is shown in Fig. 12.

The curves in Figs. 12 and 13 show the behavior of A_2(1 cm,c) vs. dopant concentration using the Beer-Lambert relation, Eq. (9). A single absorption spectrum was used to generate the curve. The agreement between the data and the curves suggests that the Beer-Lambert relation reasonably describes the concentration dependence of absorption for this case of absorbing particles in a fluid.

2) Temperature Dependence.

The measurements previously discussed were made near 200°C, except as noted. Since the anticipated temperature of the doped Hitec as a heat transfer fluid in a solar central receiver is near 500°C, one would like to know whether significant changes in solar absorption occur over this temperature range.

The shift of the Hitec absorption edge with temperature was measured using a Cary 1 mm pathlength infrasil spectrometer cell and a conventional Beckman DK-2 transmission spectrometer. The absorption edge, for measurement purposes, was arbitrarily defined as the wavelength at which the external transmission through the cell and liquid was 5% of the incident beam. The results, shown in Fig. 14, indicate that the absorption edge wavelength shifts approximately linearly to longer wavelength with increasing temperature over the range 200-500°C, typical of molten salts.[18] The increase in A_2(1 cm,0) for pure Hitec over this temperature range is approximately 1.5%.

Fluid temperatures in excess of 300°C were experimentally prohibited for spectral transmission and reflection measurements using the flow cells. Instead, the transmission through a fixed thickness of doped fluid was measured over the range 200-400°C, using an un-monochromated tungsten light source and a silicon photodetector. No differences in measured transmission were seen which would correspond to changes in A_2(1 cm,c) of more than 2%.

Based on these two experiments, no significant (> 3%) differences in A_2(1 cm,c) are expected between the data in Figs. 12 and 13 at 200°C and similar data at 500°C.

3) Light Scattering.

Diffuse transmission measurements (i.e., hemispherical minus normal) were made to indicate the extent of light scattering due to the suspended oxide particles. Typical diffuse transmission spectra are shown in Figs. 5, 6, and 7 for various dopants and concentrations, and indicate the need for the hemispherical measurements in characterizing the actual absorption. The diffuse spectra show the oxide absorption bands, and an increase in transmission with decreasing wavelength, relative to the hemispherical transmission. This latter observation indicates Rayleigh

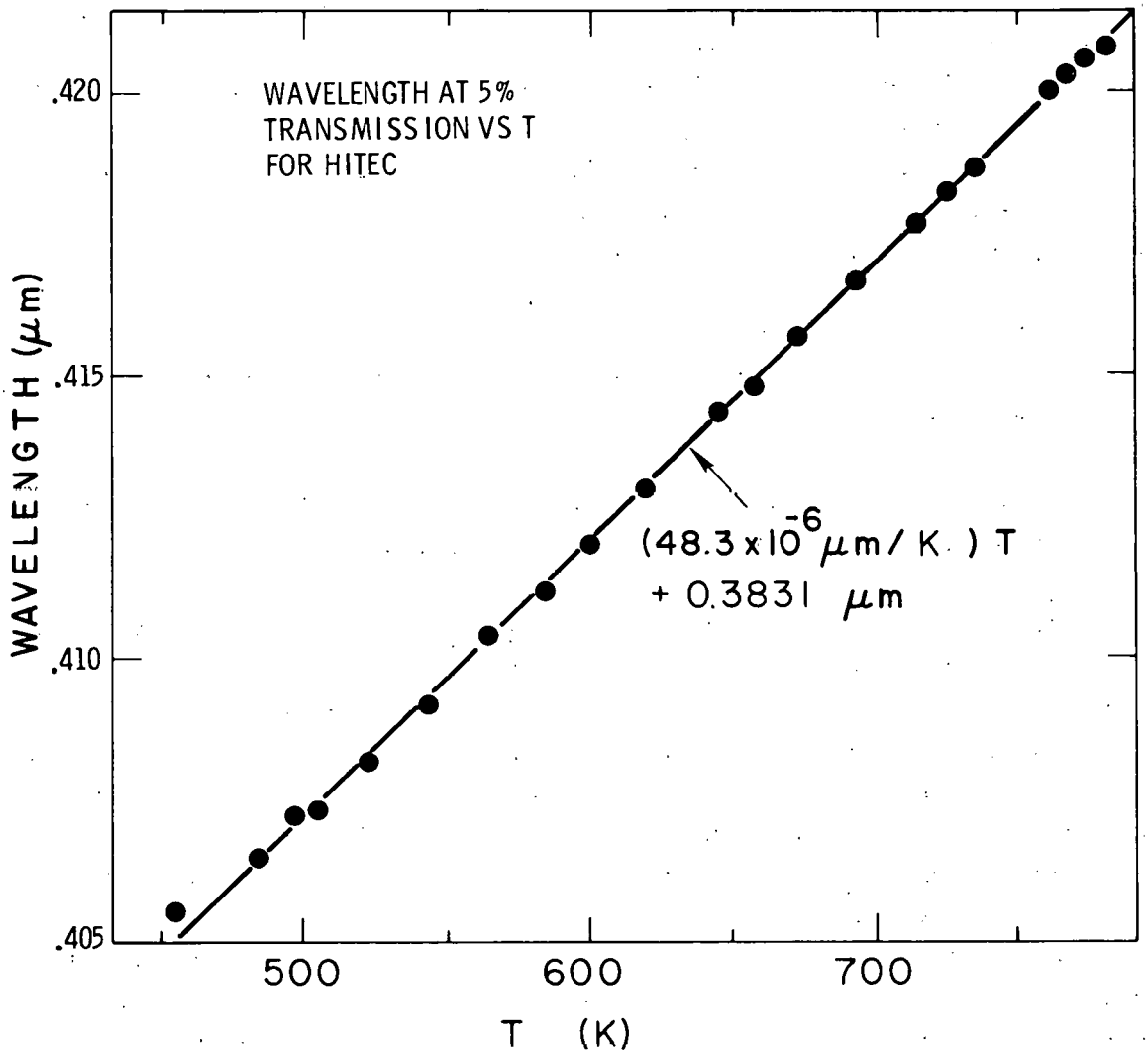

Figure 14. Fundamental absorption edge location of molten Hitec versus temperature. Edge location was arbitrarily chosen as that wavelength corresponding to 5% external transmission. Cell pathlength was 1 mm.

scattering is present, as expected by the SEM particle size estimates. A common criterion[11] for Rayleigh scattering is $X \leq 0.8$, where $X \equiv \pi D/\lambda$ and D is the particle diameter. (For Co_3O_4, for example, the ranges of particle sizes and wavelengths gives $0.05 < X < 0.8$.) Comparison of the diffuse spectra in Figs. 5 and 6 shows that the scattered (diffuse) component increases with increasing dopant concentration (particle density). Approximately 40% of the solar-averaged transmission is diffuse for 0.021 wt% cobalt nitrate in Hitec, while 66% is diffuse for 0.061 wt% dopant.

The measurement of the profile of the forward-transmitted beam is described above. Figure 15 shows the intensity distribution in the forward hemisphere for pure Hitec and for Co_3O_4 particles in Hitec (formed from 0.020 wt% cobalt nitrate). The distribution for CuO was also measured, and was essentially the same as for Co_3O_4. These distributions were obtained by differentiating the curves of transmission vs. total included angle, where each curve is normalized to the hemispherical transmission value (at $\theta = 90°$). In addition to causing absorption, the presence of oxide particles simply broadens the forward beam transmitted through the fluid.

An estimate of the amount of light scattering by the particles into the backward hemisphere was made by measuring the hemispherical reflection from a transmission cell containing either pure or doped Hitec. The hemispherical reflection from the cell and pure Hitec was consistent with reflection (specular) at the two air/glass interfaces (the glass/Hitec interfaces contribute negligible reflection). Addition of Co_3O_4 particles (0.030 wt% cobalt nitrate) in the fluid resulted in no increase in reflected light. Where the doped Hitec is non-absorbing, the reflection was again due to the two air/glass interfaces. In the regions of the Co_3O_4 absorption bands, the reflected intensity was reduced by an amount entirely consistent with absorption by the oxide in the fluid layer. Therefore, light scattering into the backward hemisphere by oxide particles appears to be negligible. This explains the agreement between measured absorption coefficients as determined from hemispherical transmission and reflection measurements.

The above results indicate that, in a hemispherical transmission experiment, incident radiation is either absorbed in the fluid, or transmitted into the forward hemisphere (i.e., detected), assuming negligible edge losses in the cell. As a result, the hemispherical transmission measurements yield an absorption coefficient α which accurately indicates the energy absorption in the fluid layer.

4) Discussion of Errors.

The uncertainty of the calculated absorption coefficient due to the propagation of random errors (particularly the uncertainty in the spectrometer measurements) was calculated for both transmission and reflection measurements. For the latter, the standard deviation of α was on the order of 8-15%. For transmission measurements, the percentage standard deviation decreases with increasing α; typical values are $\alpha \sim 0.2\ cm^{-1} \pm 12\%$ and $\alpha \sim 2.0\ cm^{-1} \pm 4\%$. The resultant uncertainty in the solar-averaged

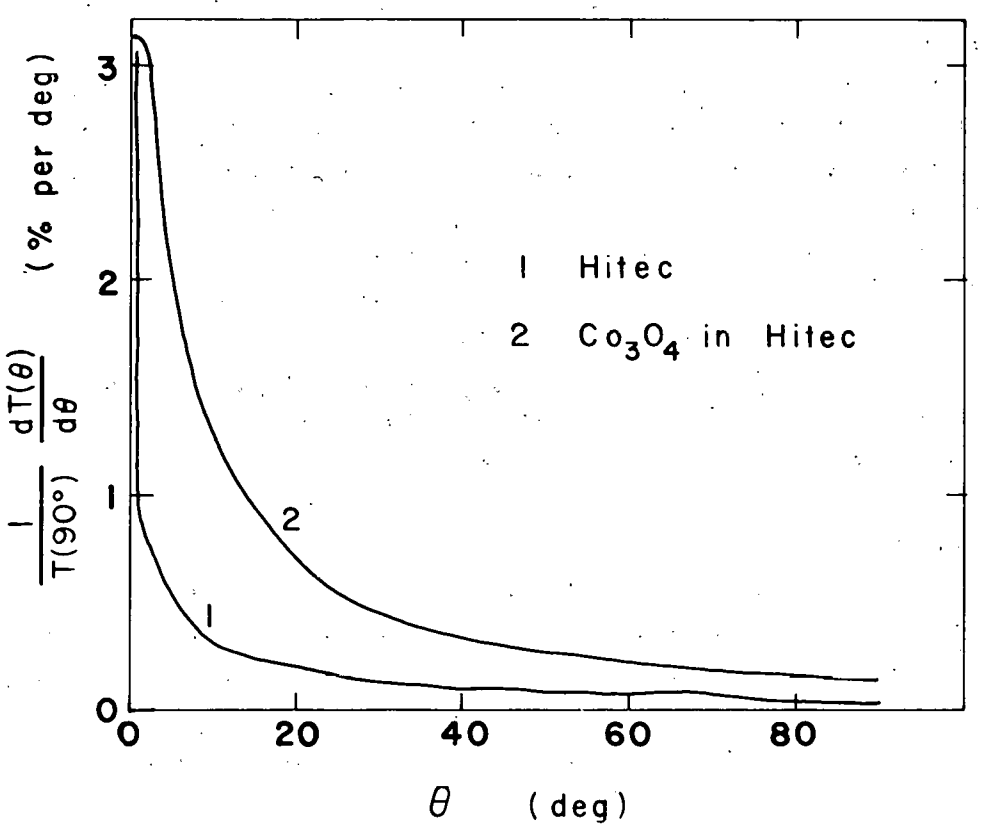

Figure 15. Transmission beam profile in the forward half-hemisphere versus θ, angle away from the normal. $\lambda = 0.6746$ μm. Cell pathlength was 6.9 mm. Dopant concentration of (2) was 0.020 wt% cobalt nitrate in Hitec. Temperature was 200°C.

absorption $A_m(x,c)$ due to uncertainties in α is less than these values. The percentage error in $A_m(x,c)$ of course depends on the magnitude of α over the whole solar spectrum; typically, values of 4-8% would be representative for the percentage uncertainty in $A_m(x,c)$.

Uncertainty in α due to systematic errors in the measurement of the fluid layer thickness were eliminated in the two-cell transmission technique, since the difference in sample and reference layer thicknesses is used, not the absolute value of each. Likewise for reflection, the calculation of α depends on the difference of the two fluid layer thicknesses, as in equation (5).

The systematic error due to the ports in the integrating sphere can be shown to be negligible.

Another possible source of systematic error in α is due to light scattering outside the detected region. For transmission measurements, this region includes the backward hemisphere, and the plane at 90° to the incident light beam (cell edges). Backward scattering was found to be negligible; similarly, light scattered out the cell edges is expected to be small, based on the angular distribution profiles, and occurs similarly for both reference and sample cells. For the reflection case, some light is scattered along the plane of the fluid layer (undetected), depending on the layer thickness. The general agreement between transmission and reflection results in this work supports the conclusion that the effects of scattering on the results are negligible.

VI. Summary

The optical absorption characteristics over the solar spectrum of an optically-doped high temperature heat transfer fluid were measured using a variety of hemispherical detection techniques. The dopants were suspensions of partially-absorbing metallic oxide particles in a eutectic molten salt fluid. The oxide of cobalt Co_3O_4 was found to have better spectral absorption characteristics than CuO particles for absorption of solar radiation. Over a range of dopant (up to ~ 0.1 wt% of hydrated metal nitrate added to the fluid), the spectral absorption coefficient of the dopant-fluid mixture was approximately linear with concentration of dopant. Solar-averaged values for the energy absorption in a fixed fluid layer were calculated for a variety of dopant concentrations. For a 1 cm layer, doping the fluid enhances the solar-absorption from 8% (pure fluid) to ~ 90% for dopant concentrations of 0.1 wt%. The solar-averaged absorption was found to vary predictably with dopant concentration, based on a Beer-Lambert dependence of absorption coefficient on concentration. Variations in solar-absorption values due to temperature variations were shown to be negligible over the 200-400°C range. The forward light scattering by the suspended particles was shown to be sufficient to necessitate hemispherical detection techniques. For a beam transmitted through a dopant-fluid layer, light scattering increased with decreasing wavelength, and

was found to broaden the transmitted beam profile in the forward direction. However, scattering in the backward hemisphere was found to be negligible.

Acknowledgements

Valuable discussions with R. B. Pettit, T. D. Brumleve, and R. C. Heckman are greatly appreciated. The author also wishes to thank G. M. Haseman for his assistance in the measurements.

References

1. V. A. Baum et al., "High-Power Solar Installations," Teploenergetika 3, 31-39 (1956).

2. A. F. Hildebrandt and L. L. Vant-Hull, "A Tower-Top Focus Solar Energy Collector," Mechanical Engineering 96, 23-27 (1974).

3. T. D. Brumleve, "A High Temperature Solar Energy System," Proceedings of the International Solar Energy Society Annual Meeting, Ft. Collins, Colorado, August 1974;

   A. C. Skinrood, T. D. Brumleve, C. T. Schafer, C. T. Yokomizo, and C. M. Leonard, Jr., Status Report on a High Temperature Solar Energy System, SAND-74-8017, Sandia Laboratories, Livermore, CA, September 1975.

4. M. Abrams, The Solar Absorptance of a Semi-Transparent Layer on an Opaque Substrate, SAND-75-8041, Sandia Laboratories, Livermore, CA, September 1975.

5. M. Abrams, The Temperature Distribution Along an Absorbing-Emitting Fluid Layer Flowing Over an Opaque Substrate, SAND-76-8622, Sandia Laboratories, Livermore, CA, May 1976.

6. K. E. Johnson and J. R. Dickinson, "High-Temperature Coordination Chemistry of Group VIII," in Advances in Molten Salt Chemistry, Vol. 2, (J. Brauenstein, G. Mamantov, and G. P. Smith, eds), Plenum Press, New York (1973).

7. D. M. Gruen, "Spectroscopy of Transition Metal Ions in Fused Salts," in Fused Salts, (B. R. Sundheim, ed), McGraw-Hill, New York (1964).

8. "DuPont Hitec® Heat Transfer Salt," E. I. DuPont de Nemours and Co., Explosives Dept., Chem. Products Sales Div., Wilmington, Delaware, 19898.

9. E. G. Bohlmann, "Heat Transfer Salt for High Temperature Steam Generation," Oak Ridge National Laboratory, ORNL-TM-3777 (1972).

10. Adelheid Kofler, Monatsh. Chem. 86, 646 (1955).

11. G. Kortum, Reflectance Spectroscopy. Principles, Methods, Applications, Springer-Verlag, New York (1969).

12. H. Jindal, PhD Thesis, Temple Univ., Philadelphia, PA, 1965, in G. Janz., Molten Salts Handbook, Academic Press (1967), p. 92.

13. H. Bloom and D. C. Rhodes, J. Phys. Chem. 60, 791 (1956).

14. D. E. Gray (ed), American Institute of Physics Handbook, Third Edition, McGraw-Hill, New York (1972).

15. W. W. Wendlandt and H. G. Hecht, Reflectance Spectroscopy, Interscience, New York (1966).

16. The source of the solar data files is Dr. M. Thekaekara, NASA-Goddard Space Flight Center.

17. E. Rhodes and A. R. Ubbelohde, Proc. Royal Soc. (London) A251, 156 (1959).

18. B. Cleaver, E. Rhodes, and A. R. Ubbelohde, Faraday Soc. Disc. 32, 22 (1961).

DISTRIBUTION:

TID-4500-R65, UC-62 (294)

U.S. Energy Research and Development
Administration
Solar Energy Division
29 Massachusetts Ave.
Washington, D.C. 20545
Attn: G. Kaplan
S. Gronich
J. Rannels
L. Melamed

Tom Tracey
Martin-Marietta
Denver Division
P. O. Box 179
Denver, Colorado

2151 R. C. Heckman
5000 A. Narath

Attn: 5100 J. K. Galt
5200 E. H. Beckner
5400 A. W. Snyder
5700 J. H. Scott

5710 C. E. Brandvold
5711 C. E. Brandvold (actg)
5712 J. A. Leonard
5713 J. V. Otts
5714 R. P. Stromberg
5715 R. H. Braasch
5719 D. G. Schueler
5800 R. S. Claassen

Attn: 5810 R. G. Kepler
5820 R. L. Schwoebel
5830 M. J. Davis

5840 H. J. Saxton

Attn: 5844 F. P. Gerstle
5845 R. J. Eagan
5846 E. K. Beauchamp

5842 J. N. Sweet
5842 R. B. Pettit
5842 G. M. Haseman
5842 W. D. Drotning (20)
5844 B. L. Butler
8111 M. Abrams
8184 A. C. Skinrood
8184 M. Brown
8184 T. D. Brumleve
8310 D. M. Schuster

3141 Technical Library (5)
3151 Technical Publications (3)
8266 Technical Library (2)

Org.	Bldg.	Name	Rec'd by*	Org.	Bldg.	Name	Rec'd by*

*Recipient must initial on classified documents.